

# An Anomaly Detection Method for Satellites Using Monte Carlo Dropout

Mohammad Amin Maleki Sadr, Yeying Zhu, *Member, IEEE*, Peng Hu, *Senior Member, IEEE*

**Abstract**—Recently, there has been a significant amount of interest in satellite telemetry anomaly detection (AD) using neural networks (NN). For AD purposes, the current approaches focus on either forecasting or reconstruction of the time series, and they cannot measure the level of reliability or the probability of correct detection. Although the Bayesian neural network (BNN)-based approaches are well known for time series uncertainty estimation, they are computationally intractable. In this paper, we present a tractable approximation for BNN based on the Monte Carlo (MC) dropout method for capturing the uncertainty in the satellite telemetry time series, without sacrificing accuracy. For time series forecasting, we employ an NN, which consists of several Long Short-Term Memory (LSTM) layers followed by various dense layers. We employ the MC dropout inside each LSTM layer and before the dense layers for uncertainty estimation. With the proposed uncertainty region and by utilizing a post-processing filter, we can effectively capture the anomaly points. Numerical results show that our proposed time series AD approach outperforms the existing methods from both prediction accuracy and AD perspectives.

**Index Terms**—Anomaly detection, telemetry time series data, satellite communications, uncertainty estimation.

## I. INTRODUCTION

Satellites are complicated systems composed of various interconnected technologies such as telemetry sensing, mobile communications, and navigation systems [1]. Proactive diagnosis of failures, anomaly detection (AD), and response to potential hazards are required to guarantee the availability and continuity of satellite services [2]. Considering the complex design structure and harsh environment of the space, AD on the satellites cannot be performed directly in the outer space; instead, the telemetry data is employed to provide healthy key information that can be used to recover the satellite from the possible problems [3]. Previous satellite AD systems were based on expert knowledge. However, by receiving a large amount of data from different telemetry channels, the expert-based (human-based) AD systems cannot properly discover anomalies, so data-driven intelligent AD methods are recommended [4].

Many studies have focused on deep neural networks (DNN) for data-based AD for spacecraft applications [5],

[6]. AD in this context has been studied from two different standpoints, which are:

1) *Forecasting-based method*: In this approach, the prediction error is computed as a difference between the current and the predicted states. Then, by leveraging a thresholding-based method, an anomaly can be detected. The idea behind this approach is that an efficient detection method should learn the expected behavior of a telemetry channel, so any deviation from the expected response can be flagged as a tentative anomaly [7]–[14].

2) *Reconstruction-based method*: In this AD approach, time series data is reconstructed, and then by comparing the real (true) and reconstructed values, anomalies are detected [15]–[18]. As this approach must reconstruct the time series to detect anomalies, it cannot be performed in real-time.

Although both reconstruction and forecasting-based approaches can capture the anomaly points, they cannot provide confidence intervals of an NN model. However, model uncertainty is essential for assessing how much to rely on the forecast produced by the model and it plays a critical role in applications like AD. The uncertainty measure can be the variance or confidence intervals around the prediction made by the NN. In this paper, we use MC dropout to capture the variance and to construct confidence interval for the NASA satellite telemetry dataset [7]. Specifically, by using MC dropout, we derive the first- and second-order statistics of an NN consisting of the LSTM cells and the dense layers. These statistics are used to determine which points fall inside the confidence region and flag tentative points that are outside the region. In this paper, we describe how to use Bayesian LSTM for fault detection, identification, and recovery (FDIR) for spacecrafts. We show the proposed MC-dropout approach outperforms the existing methods [7]–[18] and it has several advantages, which will be discussed in detail in the next sections.

The rest of this paper is organized as follows: in Section II, we present the related works and lay out our contributions. In Section III, we discuss the proposed pre-processing method. Bayesian LSTM methods for training and post-processing AD filters are presented in Section IV. Performance evaluation of the proposed AD method is presented in Section V followed by concluding remarks in Section VI.

## II. RELATED WORKS

In this section, we first review the literature on different AD methods, compare the existing works from various perspectives, and then discuss this paper's contributions.

This work was supported by the High-Throughput and Secure Networks Challenge program of National Research Council Canada under Grant No. CH-HTSN-418. Mohammad Amin Maleki Sadr and Yeying Zhu are with the Dept. of Statistics and Actuarial Science, University of Waterloo, ON N2L 3G1, Canada. Peng Hu is with Digital Technologies Research Center, National Research Council Canada and with the Dept. of Statistics and Actuarial Science, University of Waterloo, ON N2L 3G1, Canada. (Email: Peng.Hu@nrc-cnrc.gc.ca)

### A. Literature Review

While forecasting-based methods suffer from sensitivity to parameter selection and often require strong assumptions and extensive domain knowledge about the data, they grant a significant amount of interest due to their low complexity. In this respect, some statistical-based models have been proposed, such as Auto-regressive Integrated Moving Average (ARIMA), which is an analytical model that learns the time series auto-correlation for future value predictions [10]. Furthermore, different sequential based deep neural network (NN) approaches such as LSTM, DeepAR, HTM are also forecasting-based methods [12]–[14]. In [13], the authors introduce hierarchical temporal memory (HTM) for AD in streaming data. The HTM encodes the current input to a hidden state and predicts the next hidden state. In [12], the performance of LSTM for detecting anomalies in the space shuttle dataset is discussed. In [14], the authors used DeepAR which is based on autoregressive recurrent networks. In this approach, anomalies are computed as the regression errors which are the distance between the median of the predicted and the true values.

On the other hand, reconstruction-based methods aim to learn a model in order to capture the low-dimensional structure of the data. Different from the normal points, the anomalies lose more information when mapping to a lower dimensional space, so, as a result, they cannot be effectively reconstructed. Thus, the points with high reconstruction errors are more likely to be anomalies. In this respect, generative adversarial networks (GANs) for time series AD are proposed in [16], [18]. The Omni-Anomaly method in [15] proposes a stochastic recurrent neural network (RNN), which captures the normal patterns of multivariate time series by modeling data distribution through stochastic latent variables. Furthermore, in [7], the LSTM Auto-Encoder (AE) efficiency for detecting the satellite anomalies is demonstrated. Recently, in [19], the authors proposed a reconstruction-based AD method based on a combination of AE and convolutional NN to capture the temporal correlations and spatial features of the multivariate time series. In [20], an implicit neural representation-based AD approach is utilized. In [21], [22], a deep transformer NN which uses attention-based sequence encoders for AD is developed. More specifically, in [22] the prediction accuracy and AD are shown to be significantly improved by using an attention-based mechanism.

Nevertheless, both reconstruction and forecasting-based approaches are shown promising results in AD, they cannot provide a confidence region of the predicted points by NN. In the context of deep NN, the uncertainty region is defined as the likelihood interval for the true value that the NN prediction lies within, and the main approach to construct this interval is Bayesian Neural Network (BNN) [23]. Using this uncertainty region and predicted value by NN, we can determine the anomaly points. As BNN does not suffer from over-fitting and always offers uncertainty estimation, it grants a significant amount of interest in many applications [24]. However, finding the posterior distribution of BNN is challenging and computationally intractable. Therefore, the

posterior distribution needs to be approximated with different techniques [24]–[28]. Among various approximation approaches, the MC dropout has demonstrated important benefits, such as lower computational cost and higher precision, over other methods [24]. The usage of MC dropout for RNN (i.e., LSTM) and the mathematical formulation can be found in [29]. In [1], the authors proposed an AD technique based on an approximation of BNN. Furthermore, in [30], [31], application of BNN for AD is discussed. Moreover, in [32], the authors used the inference abilities and modeling characteristics of dynamic Bayesian networks in developing and implementing a innovative approach for FDIR of autonomous spacecraft.

### B. Contributions

In this subsection, we discuss the contributions, advantages, and major differences of the proposed Bayesian method compared to other competitors. The key contributions of this paper are summarized as follows:

- We propose an unsupervised Bayesian AD method for time series data. In particular, we use the MC dropout as a low-complexity approximation of BNN in both the dense and LSTM layers of the NN for AD tasks. The proposed Bayesian method not only forecasts the data accurately but also provides a confidence interval as a byproduct. Note that, our approximation of BNN is more precise than the method in [1]. The MCD-BiLSTM-VAE method in [1], uses dropout only before the dense layers rather than the entire network composed of both the LSTM cells and the dense layers, and thus it only captures the uncertainty of the dense layers. In contrast, we applied MC dropout at both of the LSTM and dense layers. Indeed, to get a precise approximation for BNN, the uncertainty of both LSTM and the dense layers should be acquired simultaneously [24], [29]. Furthermore, another significant difference between our approach and [1] in AD is that the thresholding approach in [1] is static, whereas we propose a dynamic thresholding method. For the dataset under consideration, the dynamic thresholding method surpasses the approach of [1] in terms of more accurate prediction and better classification results.
- We propose a pre-processing method, which is based on an adaptive weighted average inside a time window with a variable length to smooth the time series. In our pre-processing method, unlike the standard pre-processing steps such as normalization and data cleaning, which are implemented in [1], [7], [11], [16], [17], we first clean, normalize and scale the dataset, then implement an innovative algorithm. To the best of our knowledge, no prior work can be found that uses this method.
- The proposed Bayesian method is a low complexity approach in terms of training time and throughput. In fact, mathematically, it can be shown that the dropout itself reduces the complexity in terms of the number of operations during both of the training and testing processes [33]. Moreover, comparing to the

reconstruction-based methods such as [1], [7], [16], our method is less computationally complex since it uses a smaller portion of the time series for predicting the next step. Indeed, at each time step, we use a number of data points equal to the order of the Markov model (which in practice will generally be one or two points) to estimate the next step and detect tentative anomalies. In contrast, reconstruction-based methods utilize all the time-series samples for AD. Consequently, they cannot be implemented in the real-time.

- Our proposed method prevents the model from over-fitting, which is due to adding the regularization term to the loss function [33]. This is different from the methods in [7], [11], [16], [17], which might suffer from over-fitting.
- We propose a post-processing algorithm which is based on the divergence of a succession of predicted data points from the corresponding confidence intervals. This is different from the approaches in [1], [7], [16], which suffer from a high number of false positives. The proposed post-processing approach is shown to lessen the number of false positives and, as a result, improves the accuracy of AD.

### III. PRE-PROCESSING FOR ANOMALY DETECTION

The raw telemetry data could not be directly ingested into our AD algorithm, and it should first go through a pre-processing stage [7]. A special weighted moving average (WMA) filter is adopted to improve the prediction accuracy by making the time series smoother [34]. In our terminology, the high prediction accuracy is equivalent to low mean square error (MSE) between the real values and the predicted values. However, when there exist anomaly points inside a window of the time series, the standard WMA may not be applicable. In fact, due to the averaging operation between the current and the adjacent points, there exists a high chance of missing an anomaly point. Our motivation here is to devise a strategy to take the advantages of the WMA for improving the prediction accuracy without missing any anomaly point. In fact, we average among the consecutive data points within an adaptive rolling window with a variable length. The idea lies in the fact that when the difference between two consecutive measurements is high, there exists a high chance of having an outlier/anomaly point. Therefore, a narrower window length should be used, as we do not want the anomaly point to be missed before applying the anomaly detection algorithm. Alternatively, when the difference between two consecutive points is small, we choose a wider window to make the time series smoother. Assume that  $\mathbf{u} \in \mathbb{R}^{n \times 1}$  and  $\mathbf{x} \in \mathbb{R}^{n \times 1}$  are the raw data and the pre-processed data, respectively. Let  $l_w(k)$  be the length of the  $k$ th window of our filter. Assume that the processed data in the  $k$ th window is  $\mathbf{x}(k)$ , where  $k \in \mathcal{J}$ ,  $\mathcal{J} = \{1, \dots, n\}$ . The smoothed data is given by:

$$\mathbf{x}(k) = \frac{1}{\|\kappa\|} \sum_{i=-\frac{l_w(k)}{2}}^{\frac{l_w(k)}{2}} \alpha_i \mathbf{u}(k-i), \quad (1)$$

where  $\kappa = [\alpha_{-\frac{l_w(k)}{2}} \dots \alpha_{\frac{l_w(k)}{2}}]^T$ ,  $\|\cdot\|$  is the vector norm function, and  $\alpha_i, i \in \mathcal{I} = \{-\frac{l_w(k)}{2}, \dots, \frac{l_w(k)}{2}\}$  are the smoothed filter coefficients. In our approach, the smoothing coefficients  $0 \leq \alpha_i \leq 1$ , depend on the distance function  $\mathbf{d}$ , where  $\mathbf{d}(k-i) = |\mathbf{u}(k-i-1) - \mathbf{u}(k-i)|$ . The distance function is the absolute difference between two successive data points inside the  $k$ th window. In this pre-processing algorithm, we start with  $l_w(0) = 2$  and  $\alpha_0 = 1$ . Let the distance threshold value be  $d_{th}^{(k)} = m^{(k)} + 2\sigma^{(k)}$ , where  $m^{(k)}$  and  $\sigma^{(k)}$  are the mean and standard deviation (s.t.d.) of the data inside the  $k$ th window. We choose the threshold value  $d_{th}^{(k)} = m^{(k)} + 2\sigma^{(k)}$  to take into account both the mean and variance inside each window. However, this threshold can be further improved by examining the exact distribution of different time series and choosing the optimal value for the threshold. It remains an interesting avenue for our future studies.

For the  $i$ th data in the  $k$ th window, if  $\mathbf{d}(k-i) < d_{th}^{(k)}$  (i.e., we do not see a sudden change), we increase the window length and set  $\alpha_i = 1$ ,  $i \in \mathcal{I}$ . Otherwise, if  $\mathbf{d}(k-i) \geq d_{th}^{(k)}$ , we have

$$\alpha_i = \begin{cases} 0 & i \in \mathcal{I} - \{0\} \\ 1 & i = 0, \end{cases} \quad (2)$$

then we increment  $k$ , and proceed to another window, i.e.,  $k = k + 1$ . The pre-processing procedure is shown in Algorithm 1.

---

#### Algorithm 1 Pre-processing algorithm

---

**Input:**  $\mathbf{u}(k)$ .

**Output:**  $\mathbf{x}(k)$ .

- 1: Initialization:  $l_w(0) = 2$ ,  $\alpha_0 = 1$ ,  $k = 0$ .
  - 2: **while**  $k \leq n$  **do**
  - 3:     Calculate the mean  $m^{(k)}$  and s.t.d.  $\sigma^{(k)}$  of the values inside the  $k$ th windows with length  $l_w(k)$ .
  - 4:     Select the  $k$ th threshold as  $d_{th}^{(k)} = m^{(k)} + 2\sigma^{(k)}$
  - 5:     **for**  $i \in \mathcal{I}$  **do**
  - 6:         **if**  $\mathbf{d}(k-i) < d_{th}^{(k)}$  **then**
  - 7:              $\alpha_i = 1$
  - 8:              $l_w(k) = l_w(k) + 1$
  - 9:         **else if**  $\mathbf{d}(k-i) > d_{th}^{(k)}$  **then**
  - 10:             Break
  - 11:         **end if**
  - 12:     **end for**
  - 13:     Calculate  $\mathbf{x}(k) = \frac{1}{\|\kappa\|} \sum_{i=-\frac{l_w(k)}{2}}^{\frac{l_w(k)}{2}} \alpha_i \mathbf{u}(k-i)$ .
  - 14:     Go to the next window, i.e.,  $k = k + 1$ .
  - 15: **end while**
- 

### IV. BAYESIAN LSTM METHOD FOR PREDICTION AND UNCERTAINTY ESTIMATION

Here, we discuss a Bayesian LSTM approach for predicting the mean of the model and its associated variance (uncertainty level). Fig. 1 shows our proposed NN model and the underlying Bayesian approach, where we use several

LSTM cells followed by the dense layers. In this section, we adopt the MC dropout for approximation of the BNN model in both of the LSTM and dense layers separately.

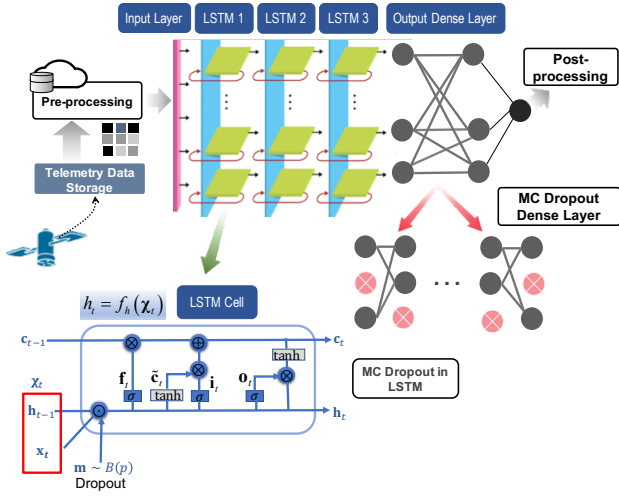


Figure 1: An illustration of the proposed system model using Bayesian LSTM

#### A. MC dropout as an approximation of BNN

We assume an NN with  $L$  LSTM and  $D$  dense layers. A batch of  $T$  observations is passed through the input layer. By assuming  $T_D$  as the length of the  $D$ th dense layer, we denote  $\mathbf{x} \in \mathbb{R}^T$  and  $\mathbf{y} \in \mathbb{R}^{T_D}$  as the input and output of NN, respectively. Assume that  $\omega$  with prior distribution  $p(\omega)$  represents a collection of the NN parameters. The probability of the output vector given the data for an associated input vector  $\mathbf{x}$  is:

$$p(\mathbf{y} | \mathbf{x}, \mathbf{D}) = \mathbb{E}_{p(\omega | \mathbf{D})} (p(\mathbf{y} | \mathbf{x}, \omega)), \quad (3)$$

where  $\mathbf{D} = \{(x_t, y_t) \forall t \in \{1, \dots, T\}\}$  and  $p(\omega | \mathbf{D})$  are a batch of data, and the posterior distribution on weights, respectively. The expectation under  $p(\omega | \mathbf{D})$  is equivalent to using an ensemble of an infinite number of models, which is indeed computationally intractable.

One feasible solution is to approximate the posterior distribution over the model parameters  $p(\omega | \mathbf{D})$  with a simpler distribution  $q(\omega)$ . A metric of similarity (or distance) between two probability distribution functions (PDF) is Kullback-Leibler (KL) divergence. Here, we minimize the  $\text{KL}(q(\omega) || p(\omega | \mathbf{D}))$  which is the KL distance between  $p(\omega | \mathbf{D})$  and  $q(\omega)$  [24]. More specifically, we solve the following optimization problem:

$$\min_{q(\omega)} \text{KL}(q(\omega) || p(\omega | \mathbf{D})), \quad (4)$$

which is equal to minimizing the following:

$$\min_{q(\omega)} - \int q(\omega) \log p(\mathbf{y} | \mathbf{x}, \omega) d\omega + \text{KL}(q(\omega) || p(\omega)). \quad (5)$$

where  $p(\omega)$  stands for the prior distribution of the NN parameters. As seen in (5), the objective function is composed of two parts. The first component is the NN loss

function and the second one stands for the regularization effect, which prevents the model from being over-fitted. Minimizing the second component is equivalent to finding a  $q(\omega)$  close to the prior, which essentially avoids over-fitting. The first component, on the other hand, can be rewritten with the MC sampling over  $\omega$  with a single sample as the following:

$$- \frac{1}{T} \sum_{n=1}^T \int \log p(\mathbf{y}_n | f^\omega(\mathbf{x}_n)) d\omega. \quad (6)$$

In the next subsection, we discuss the detailed structure of the function  $f^\omega(\mathbf{x}_n)$  in (6) using different layers of LSTM followed by dense layers.

#### B. Application of MC dropout for approximation of the posterior distribution of NN parameters

As shown in Fig. 1, a simple LSTM unit contains input, output, and additional control gates. The following formulation briefly shows the principle of the LSTM [35]:

$$\begin{aligned} \mathbf{i}_t &= \sigma(\mathbf{W}_i \chi_t + \mathbf{b}_i), & \mathbf{f}_t &= \sigma(\mathbf{W}_f \chi_t + \mathbf{b}_f), \\ \mathbf{o}_t &= \sigma(\mathbf{W}_o \chi_t + \mathbf{b}_o), & \tilde{\mathbf{c}}_t &= \tanh(\mathbf{W}_c \chi_t + \mathbf{b}_c), \\ \mathbf{c}_t &= \mathbf{f}_t \odot \mathbf{c}_{t-1} + \mathbf{i}_t \odot \tilde{\mathbf{c}}_t, & \mathbf{h}_t &= \mathbf{o}_t \odot \tanh(\mathbf{c}_t), \end{aligned} \quad (7)$$

where  $\chi_t = [\mathbf{x}_t \ \mathbf{h}_{t-1}]^T$  and  $\mathbf{x}_t$  represents the input data,  $\sigma$  is the logistic sigmoid function and  $\odot$  is the element-wise product. Also,  $\mathbf{c}_t$  represents the state value of the LSTM unit (while  $\tilde{\mathbf{c}}_t$  is the candidate state value),  $\mathbf{i}_t$  stands for the state value of the input gate,  $\mathbf{f}_t$  represents the state value of the forget gate,  $\mathbf{o}_t$  is the state value of the output gate,  $\mathbf{h}_t$  is the output of the LSTM unit, and  $t$  is the current time step.  $\mathbf{W}$  and  $\mathbf{b}$  are the corresponding weight and bias parameters at each of the aforementioned gates in (6). According to the aforementioned formulation of LSTM, the following mapping function can be concluded (omitting the bias parameter):

$$\mathbf{h}_t = f_h(\chi_t). \quad (8)$$

By applying a dropout at the input and hidden layers, we have [29]:

$$\mathbf{i}_t = \sigma(\mathbf{W}_i(\chi_t \odot \mathbf{m}) + \mathbf{b}_i), \quad (9)$$

$$\mathbf{f}_t = \sigma(\mathbf{W}_f(\chi_t \odot \mathbf{m}) + \mathbf{b}_f), \quad (10)$$

$$\mathbf{o}_t = \sigma(\mathbf{W}_o(\chi_t \odot \mathbf{m}) + \mathbf{b}_o), \quad (11)$$

$$\tilde{\mathbf{c}}_t = \tanh(\mathbf{W}_c(\chi_t \odot \mathbf{m}) + \mathbf{b}_c), \quad (12)$$

$$\mathbf{c}_t = \mathbf{f}_t \odot \mathbf{c}_{t-1} + \mathbf{i}_t \odot \tilde{\mathbf{c}}_t, \quad (13)$$

where  $\mathbf{m} \sim \mathcal{B}(p)$  is a random mask vector where each row has a Bernoulli distribution with the parameter  $p$  and it is repeated at all the time steps. We use the MC dropout in the dense layers by dropping the neurons randomly according to the Bernoulli distribution during the testing phase. For the  $k$ th dense layer, we have [24]:

$$\mathbf{W}_k = \text{diag}([z_{k,j}]_{j=1}^{K_i}) \mathbf{M}_k, \quad (14)$$

$$z_{k,j} \sim \mathcal{B}(p_k) \quad \forall k \in \{1, \dots, D\}, j \in \{1, \dots, K_{k-1}\},$$

where  $p_k$  and matrix  $\mathbf{M}_k$  of dimensions  $K_k \times K_{k-1}$  are the variational parameters. The binary variable  $z_{k,j} = 0$  corresponds to the unit  $j$  in layer  $k-1$  being dropped out as an input to the  $k$  layer. By assuming  $\mathbf{b}_k$  as a bias at the  $k$ th dense layer, the weight matrix (NN parameter) can be considered as  $\omega = [\mathbf{W}_k, \mathbf{W}_i, \mathbf{W}_f, \mathbf{W}_o, \mathbf{W}_{\bar{c}}, \mathbf{b}_k, \mathbf{b}_i, \mathbf{b}_f, \mathbf{b}_o, \mathbf{b}_c]^T$ . Therefore, (6) is rewritten as

$$\sum_{i=1}^N \log(p(y_i | \sqrt{\frac{1}{K_D}} \hat{\mathbf{W}}_D \sigma(\dots \sqrt{\frac{1}{K_2}} \hat{\mathbf{W}}_2 \sigma(\hat{\mathbf{W}}_1(\psi_T) + \mathbf{b}_1) \dots))), \quad (15)$$

where  $\psi_T \triangleq [\mathbf{x}_{T,i}, f_h^{\hat{\omega}}(\dots f_h^{\hat{\omega}}([\mathbf{x}_{0,i}, \mathbf{h}_0])]$ , and  $\hat{\omega} \sim q(\omega)$ . For each sequence  $\mathbf{x}_i$ , we sample a new realization  $\hat{\omega} = [\hat{\mathbf{W}}_k, \hat{\mathbf{W}}_i, \hat{\mathbf{W}}_f, \hat{\mathbf{W}}_o, \hat{\mathbf{W}}_{\bar{c}}, \hat{\mathbf{b}}_k, \hat{\mathbf{b}}_i, \hat{\mathbf{b}}_f, \hat{\mathbf{b}}_o, \hat{\mathbf{b}}_c]^T$ . Each symbol in the sequence  $\mathbf{x}_i = [\mathbf{x}_{i,1}, \dots, \mathbf{x}_{i,T}]^T$  is passed through the function  $f_h^{\hat{\omega}}$  with the same weight realizations  $\hat{\omega}$  used at the time step  $t \leq T$ . In the dense layers, and LSTM layers, the MC dropout is performed during both of the training and testing phases. To summarize, in MC dropout, we set the input of each neuron (or LSTM cell) independently to zero with probability  $p$ , which means running the network several times with different random seeds. Algorithm 2 shows the different steps of the MC dropout approach.

---

**Algorithm 2** MC dropout algorithm
 

---

Repeat:

Sample  $z_{i,j} \sim \mathcal{B}(p_i)$ ,  $i \in \{1, \dots, D\}$ ,  $j \in \{1, \dots, K_{i-1}\}$ , and  $\mathbf{m} \sim \mathcal{B}(p_k) \quad \forall k \in \{1, \dots, L\}$  and set (12), (13), (14), (15), (16), (17), respectively, and find  $\hat{\omega} = [\hat{\mathbf{W}}_k, \hat{\mathbf{W}}_i, \hat{\mathbf{W}}_f, \hat{\mathbf{W}}_o, \hat{\mathbf{W}}_{\bar{c}}, \hat{\mathbf{b}}_k, \hat{\mathbf{b}}_i, \hat{\mathbf{b}}_f, \hat{\mathbf{b}}_o, \hat{\mathbf{b}}_c]$  where  $\hat{\omega} \sim q(\omega)$ .

Minimize (one step):

$$- \int q(\omega) \log(p(\mathbf{y} | \mathbf{x}, \omega)) + \text{KL}(q(\omega), p(\omega)).$$


---

Assume that we have  $l$  sets of realization of the NN after applying the MC dropout, as shown in Fig. 1. As derived in [24], the approximated predictive distribution is given by the following:

$$q(\mathbf{y} | \mathbf{x}) = \int p(\mathbf{y} | \mathbf{x}, \omega) q(\omega) d\omega \quad (16)$$

The first two moments are derived as [24]:

$$\mathbb{E}_{q(\mathbf{y} | \mathbf{x})}(\mathbf{y}) \approx \frac{1}{l} \sum_{t=1}^l \mathbb{E}(\mathbf{y} | \mathbf{x}, \omega^t) \quad (17)$$

and

$$\mathbb{E}_{q(\mathbf{y} | \mathbf{x})}(\mathbf{y}^T \mathbf{y}) \approx \frac{1}{l} \sum_{t=1}^l \mathbb{E}(\mathbf{y} | \mathbf{x}, \omega^t)^T \mathbb{E}(\mathbf{y} | \mathbf{x}, \omega^t) \quad (18)$$

The model's predictive variance is

$$\text{Var}_{q(\mathbf{y} | \mathbf{x})}(\mathbf{y}) = \mathbb{E}_{q(\mathbf{y} | \mathbf{x})}(\mathbf{y}^T \mathbf{y}) - \mathbb{E}_{q(\mathbf{y} | \mathbf{x})}(\mathbf{y})^T \mathbb{E}_{q(\mathbf{y} | \mathbf{x})}(\mathbf{y}) \quad (19)$$

### C. Post-processing of AD

To reduce the number of false positives, we propose a post-processing algorithm, which is based on the deviation of a sequence of predicted data points from the confidence region. More specifically, if a predicted data point is outside the uncertainty region of the MC dropout, then it is considered as a tentative anomaly point. In our specific dataset, anomaly points do not occur as a single point; instead, they emerge as a sequence (burst) of dependent points in a particular part of the time series.

It is important to determine a time when the anomaly starts. Let  $N_{max}$  be a range of consecutive data points in time series. In our approach, if  $0.8N_{max}$  of the consecutive points are outside the confidence region simultaneously, then we consider the first index of the sequence as the starting point of the anomaly sequence. For this specific dataset, this post-processing approach can significantly reduce the number of false positives. Choosing a suitable value for  $N_{max}$  depends on the maximum allowable delay. We can improve the accuracy if we wait for more sample points to announce the anomaly; however, successful alert with a huge delay is not useful. Therefore, if an AD algorithm raises an alert fast enough (i.e., before a maximum allowable delay) the whole anomaly fragment is considered to be detected successfully. We will further illustrate this method in numerical results.

## V. NUMERICAL RESULTS

First, we describe the methodology for evaluating AD, then summarize the specific dataset under consideration, followed by the performance evaluation. The source code is available at <https://bit.ly/3zf1Ipb>.

### A. Methodology

We assume an NN with 3 LSTM and 2 dense layers, where the MC dropout rate is assumed to be 0.2. We adopt PyTorch, an open-source framework for machine learning, to implement our proposed approach. We use the dataset in [7] to compare and evaluate our method with the following approaches: i) dynamic thresholding approach with LSTM Auto-Encoder (AE) [7]; ii) TadGan approach [16]; iii) MadGan method [17]; iv) Arima method [10]; v) LSTM method [11]; and vi) A modified version of MCD-BiLSTM-VAE method in [1] after applying the post-processing filter which has been proposed in Section IV.C. We will use the following metrics to evaluate the performance of various models: mean squared error (MSE),  $F_1$  score, accuracy, recall, and precision. Moreover, we will compare the computational complexity of different methods. These metrics have been widely used in the literature and are discussed in detail in [36].

### B. NASA dataset

We use the satellite telemetry dataset, which was originally collected by NASA [7]. The dataset comes from two spacecrafts: the Soil Moisture Active Passive (SMAP) and the Curiosity Rover on Mars (MSL). There are 82 signals

available in the NASA dataset, which are summarized in Table I. We found 54 of the 82 signals (multivariate time series) are continuous, and the remaining are discrete. There are a total of  $n$  rows corresponding to the number of timestamps or readings taken for that signal ( $n$  differs in different signals). Each sample of the data consists of one column of telemetry signal and several columns of commands. The command features are encrypted and can barely be used. Furthermore, we also found that the correlation between the command features and telemetry signals is negligible. We consider only the time series sequences from the telemetry signals in our evaluation. Therefore, the input signal to our model is an  $n \times 1$  matrix.

Table I: NASA telemetry dataset summary

Dataset	Signals	Anomaly Sequences	Data Points	Anomaly Points
SMAP	55	67	562800	54696
MSL	27	36	132046	7766

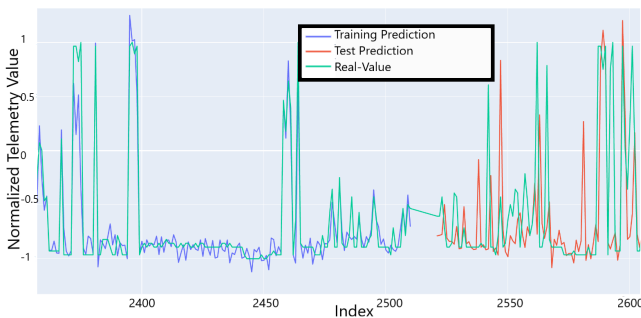


Figure 2: Examples of real values and predictions in training and testing modes for ‘F-7’ signal

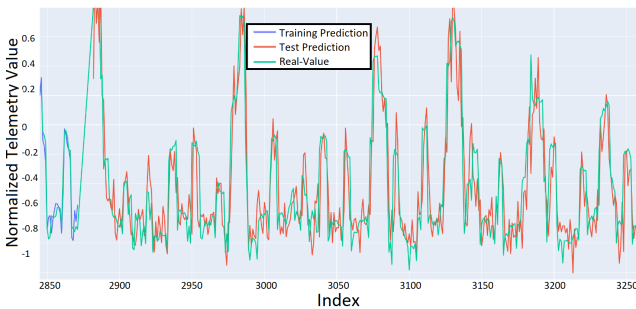


Figure 3: Examples of real values and predictions in training and testing modes for ‘P-1’ signal

### C. Evaluation

In this subsection, we evaluate and compare the proposed model with those of other studies. The comparison results between the predicted and real values in the training and testing phases for one of the MSL satellite telemetry signals i.e., ‘F-7’, and another SMAP satellite signal, i.e., ‘P-1’ are shown in Fig. 2 and Fig. 3, respectively. By analysing these two figures, we notice that our Bayesian LSTM approach

performs better on the SMAP data in the prediction phase. To show the uncertainty region by our Bayesian approach, Fig. 4 and Fig. 5 are depicted. These figures show the MC dropout bounds and corresponding predicted values for ‘F-7’ from MSL dataset and ‘P-1’ from SMAP dataset, respectively. We found that, on average, for both datasets, 84% of the predicted values are inside the uncertainty bounds. Furthermore, we use the following evaluation measures to assess our method:

1) *Mean Squared Error*: MSE, which is used as a metric for comparing forecasting-based methods, assesses the average squared difference between the real and predicted values. It is defined as  $MSE = \frac{1}{N} \sum_{i=1}^N (y_i - \hat{y}_i)^2$ , where  $\hat{y}_i$  is the predicted value at the  $i$ th timestamp. The MSE results for the two datasets for our approach, the Arima method [10], and the LSTM method [11] can be found in Table II. The MSE can be used just for forecasting-based methods, and for the reconstruction-based methods such as TadGan and MadGan, LSTM AE, it cannot be calculated. Indeed, what they calculated is the quantity of error for reconstructing the time series and it is different from the concept of MSE considered in the forecasting-based approaches. Due to the fundamental difference in definitions, we have not compare the mentioned methods with our approach.

Table II: MSE comparison of forecasting-based approaches

Baseline	Bayesian LSTM	Arima [10]	LSTM [11]
SMAP	0.05	0.61	0.07
MSL	0.21	0.83	0.29

2) *Recall*: This is often used as a sensitivity metric. It is the proportion of relevant instances that were retrieved. i.e.,  $\theta = \frac{TP}{TP+FN}$ . where  $TP$ ,  $FP$ ,  $FN$ , and  $TN$  stand for true positive, false positive, false negative, and true negative, in the confusion matrix, respectively.

3) *Precision*: It is the fraction of relevant instances among the retrieved instances, i.e.,  $\xi = \frac{TP}{TP+FP}$ .

4) *Accuracy*: It is one of the important classification performance measures. Based on the definition, it is the proportion of correct predictions (both true positives and negatives) among the total number of explored cases, i.e.,  $Accuracy = \frac{TP+TN}{TP+TN+FP+FN}$ .

5) *F<sub>1</sub> score*: This score is defined as the harmonic mean of precision and recall, i.e.,  $F_1 = \left( \frac{\xi^{-1} + \theta^{-1}}{2} \right)^{-1}$ .

For finding the best value of  $N_{max}$  in post-processing, we perform a grid search among different values of  $N_{max}$  for each signal independently and pick the optimal value in such a way that the dissimilarity between the predicted labels and the known labels is minimized. The value of  $N_{max}$  depends on the maximum allowable delay, and selecting a higher value for  $N_{max}$ , causes a smaller value for  $FP$ . Alternatively, choosing a high value for  $N_{max}$  (e.g., 100) leads to a high value for  $FN$ . Therefore, finding the optimal value for this parameter will boost the AD overall performance. Assume a new metric  $\rho_n = TP_n + TN_n - FP_n - FN_n$ . We choose  $N_{max}$  in such a way that  $\rho_n$  gets maximized within

a reasonable range of  $n$ . Fig. 6 shows the normalized value of different measurement criteria versus  $N_{max}$  for signal ‘P-1’. This figure shows that after a specific amount of  $N_{max}$ , the value of  $\rho_n$  (and other evaluation criteria) does not change. For this specific signal, the optimal value for  $N_{max}$  is  $N_{max}^{opt} = 8$ . Also, we found that the anomalies cannot be detected using some signals (e.g., ‘‘M6’’ in the MSL dataset has a value of -1 in all training and testing phases, which makes it impossible to be used in uni-variate AD cases). We have excluded these types of signals (i.e., ‘‘M6, E3, A1, D1, D3, D4, G1, D5, D11, G6, R1, A6, F3, M2, P10, M3, D16, P15, P11, P14’’ in our comparison results.

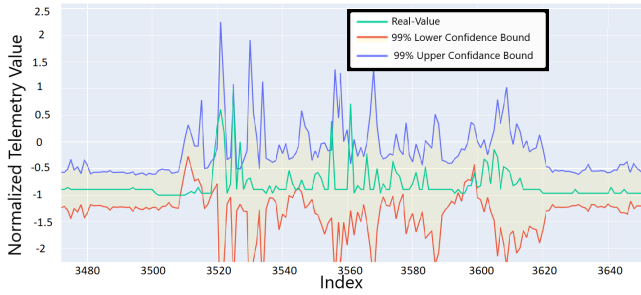


Figure 4: Uncertainty region using MC dropout for ‘F-7’ signal

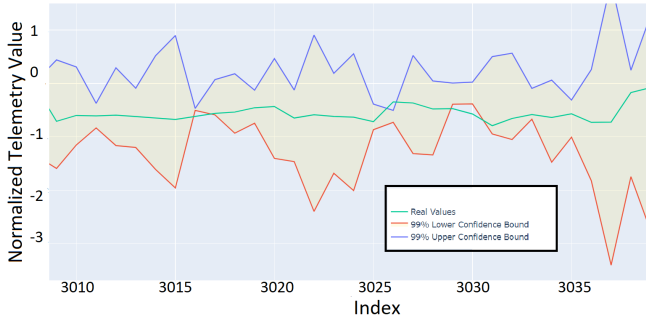


Figure 5: Uncertainty region using MC dropout for ‘P-1’ signal

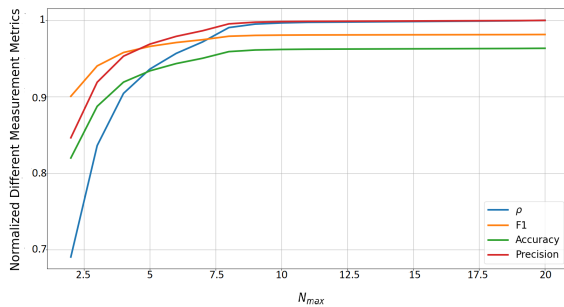


Figure 6: The normalized measurement scores v.s.  $N_{max}$  for signal ‘P-1’ to show the post-processing effect.

Table III: F1 score comparison

Baseline	Bayesian LSTM	TadGan [16]	Arima [10]	LSTM AE [7]	MadGan [17]	LSTM [11]	MCD-BiLSTM-VAE [1]
SMAP	0.84	0.66	0.42	0.69	0.12	0.62	0.67
MSL	0.74	0.55	0.49	0.55	0.11	0.48	0.64

Table IV: Comparison of learnable parameters, training time, and inference throughput

Methods	Parameters	Training Time (per epoch)	Throughput
Bayesian LSTM	229409	1.48 sec	$0.57 \times 10^3$ predictions/sec
TadGan [16]	447189	78 sec	$0.27 \times 10^2$ predictions/sec
Arima [10]	17	1.1 sec	$2.1 \times 10^3$ predictions/sec
LSTM AE [7]	86250	1.84 sec	$1.16 \times 10^3$ predictions/sec
LSTM [11]	229409	1.48 sec	$1.1 \times 10^3$ predictions/sec
MCD-BiLSTM-VAE [1]	580993	6.96 sec	$0.032 \times 10^3$ predictions/sec

In Table III, we compare the  $F_1$  score for the aforementioned methods for two different baselines. As the comparison results show, our proposed method outperforms the existing methods for AD. The closest methods to our Bayesian LSTM method in the  $F_1$  score are TadGan, LSTM AE and MCD-BiLSTM-VAE. The difference between the  $F_1$  score of our Bayesian LSTM method (and also other methods), and the MadGan approach is significant. For this reason, we have excluded the MadGan approach from the rest of the comparisons. We notice that applying the proposed post-processing approach in Section IV.C to MCD-BiLSTM-VAE method significantly improves the  $F_1$  score of the original method in [1]; thus we use a modified version of [1] in our comparisons. In addition to  $F_1$  score improvement, our method still has other advantages over TadGan, LSTM AE, LSTM, and MCD-BiLSTM-VAE approaches, which have been discussed in Section I. One of the distinct advantages is the complexity reduction of our Bayesian approach compared to other methods (e.g., TadGan).

Now let us examine the complexity cost of different methods in detail. Table IV shows the computational cost of our proposed approach compared with other methods. The reported results are performed using the free Google Colaboratory platform with 2-Core Xeon 2.2GHz, 13GB RAM and the PyTorch framework installed. The comparison results show that the Arima method performs best regarding computational complexity. While the computational complexity of our method is significantly lower than that of the TadGan approach, it is almost similar to the Arima method. Furthermore, the training time of our method is identical to the LSTM approach. This is because the MC dropout does not affect the NN during the training phase. Instead, during the testing phase, applying the dropout enables us to approximate the original BNN. Moreover, the complexity cost of MCD-BiLSTM-VAE method is higher than our approach.

Furthermore, in Table V, we compare the precision, recall, and accuracy of our method with other approaches. Considering the trade-off between complexity and performance measures, the results of the comparison show, our

Table V: Comparison of accuracy, precision, and recall

Methods	SMAP			MSL		
	Accuracy	Precision	Recall	Accuracy	Precision	Recall
Bayesian LSTM	<b>0.75</b>	<b>0.82</b>	<b>0.87</b>	<b>0.7</b>	<b>0.74</b>	<b>0.87</b>
TadGan [16]	0.76	0.76	0.69	0.58	0.58	0.68
Arima [10]	0.52	0.61	0.57	0.49	0.63	0.45
LSTM AE [7]	0.73	0.76	0.75	0.55	0.65	0.66
LSTM [11]	0.67	0.56	0.73	0.53	0.52	0.67
MCD-BiLSTM-VAE [1]	0.65	0.68	0.78	0.60	0.58	0.84

method outperforms the various competitors.

## VI. CONCLUSIONS

The proposed NN-based method provides a generic low-complexity, and prediction-based solution to advancing AD. Our method improves the MSE, precision, recall, accuracy, and  $F_1$  score compared to existing methods. The techniques proposed for LSTM can be considered a generic time series analytics tool for autonomous FDIR tasks of satellite missions. Equally important, the proposed method addresses a critical challenge in FDIR: how to efficiently use the time series data without labels to facilitate FDIR missions. The proposed work enables efficient utilization and analysis of the time series data for satellite telemetry and other FDIR applications where on-board hardware and software AD is needed.

## REFERENCES

- [1] J. Chen, D. Pi, Z. Wu *et al.*, "Imbalanced satellite telemetry data anomaly detection model based on bayesian lstm," *Acta Astronautica*, vol. 180, pp. 232–242, 2021.
- [2] E.-H. Li, Y.-Z. Li, T.-T. Li *et al.*, "Intelligent analysis algorithm for satellite health under time-varying and extremely high thermal loads," *Entropy*, vol. 21, no. 10, p. 983, 2019.
- [3] H. Safaeipour, M. Forouzanfar, and A. Casavola, "A survey and classification of incipient fault diagnosis approaches," *J. Process Control*, vol. 97, pp. 1–16, 2021.
- [4] D. Cayrac, D. Dubois, and H. Prade, "Handling uncertainty with possibility theory and fuzzy sets in a satellite fault diagnosis application," *IEEE Trans. Fuzzy Syst.*, vol. 4, no. 3, pp. 251–269, 1996.
- [5] M. Schwabacher, N. Oza, and B. Matthews, "Unsupervised anomaly detection for liquid-fueled rocket propulsion health monitoring," *J. Aeros. Comp. Inf. Com.*, vol. 6, no. 7, pp. 464–482, 2009.
- [6] S. K. Ibrahim, A. Ahmed, M. A. E. Zeidan *et al.*, "Machine learning techniques for satellite fault diagnosis," *Ain Shams Engineering Journal*, vol. 11, no. 1, pp. 45–56, 2020.
- [7] K. Hundman, V. Constantinou, C. Laporte *et al.*, "Detecting spacecraft anomalies using LSTMs and nonparametric dynamic thresholding," in *24th Proc. ACM SIGKDD Int. Conf. Knowl. Discov. Data Min.*, 2018, pp. 387–395.
- [8] N. Ding, H. Gao, H. Bu *et al.*, "Multivariate-time-series-driven real-time anomaly detection based on bayesian network," *Sensors*, vol. 18, no. 10, p. 3367, 2018.
- [9] V. Chandola, A. Banerjee, and V. Kumar, "Anomaly detection: A survey," *ACM Computing Surveys (CSUR)*, vol. 41, no. 3, pp. 1–58, 2009.
- [10] E. H. Pena, M. V. de Assis, and M. L. Proença, "Anomaly detection using forecasting methods arima and hwd," in *32nd Int. Conf. Chil. Comput. Sci. Soc. SCCC (SCCC)*. IEEE, 2013, pp. 63–66.
- [11] I. Tinawi, "Machine learning for time series anomaly detection," Ph.D. dissertation, Massachusetts Institute of Technology, 2019.
- [12] P. Malhotra, L. Vig, G. Shroff *et al.*, "Long short term memory networks for anomaly detection in time series," in *23rd European Symposium on Artificial Neural Networks, ESANN 2015, Bruges, Belgium, April 22-24, 2015*, 2015. [Online]. Available: <https://www.esann.org/sites/default/files/proceedings/legacy/es2015-56.pdf>
- [13] S. Ahmad, A. Lavin, S. Purdy *et al.*, "Unsupervised real-time anomaly detection for streaming data," *Neurocomputing*, vol. 262, pp. 134–147, 2017.
- [14] D. Salinas, V. Flunkert, J. Gasthaus *et al.*, "Deepar: Probabilistic forecasting with autoregressive recurrent networks," *International Journal of Forecasting*, vol. 36, no. 3, pp. 1181–1191, 2020.
- [15] Y. Su, Y. Zhao, C. Niu *et al.*, "Robust anomaly detection for multivariate time series through stochastic recurrent neural network," in *Proc. 25th ACM SIGKDD Int. Conf. Knowl. Discov. Data Min.*, 2019, pp. 2828–2837.
- [16] A. Geiger, D. Liu, S. Alnegheimish *et al.*, "Tadgan: Time series anomaly detection using generative adversarial networks," in *IEEE Int. Conf. Big Data*. IEEE, 2020, pp. 33–43.
- [17] D. Li, D. Chen, B. Jin *et al.*, "Mad-gan: Multivariate anomaly detection for time series data with generative adversarial networks," in *Int. Conf. Artificial Neural Netw.*, 2019, pp. 703–716.
- [18] S. Liu, B. Zhou, Q. Ding *et al.*, "Time series anomaly detection with adversarial reconstruction networks," *IEEE Transactions on Knowledge and Data Engineering*, pp. 1–1, 2022.
- [19] T. Choi, D. Lee, Y. Jung *et al.*, "Multivariate time-series anomaly detection using seqvae-cnn hybrid model," in *2022 International Conference on Information Networking (ICOIN)*. IEEE, 2022, pp. 250–253.
- [20] K.-J. Jeong and Y.-M. Shin, "Time-series anomaly detection with implicit neural representation," *arXiv preprint arXiv:2201.11950*, 2022.
- [21] S. Tuli, G. Casale, and N. R. Jennings, "Tranad: Deep transformer networks for anomaly detection in multivariate time series data," *arXiv preprint arXiv:2201.07284*, 2022.
- [22] L. Yang, Y. Ma, F. Zeng *et al.*, "Improved deep learning based telemetry data anomaly detection to enhance spacecraft operation reliability," *Microelectronics Reliability*, vol. 126, p. 114311, 2021.
- [23] A. Loquercio, M. Segu, and D. Scaramuzza, "A general framework for uncertainty estimation in deep learning," *IEEE Robot. Autom. Lett.*, vol. 5, no. 2, pp. 3153–3160, 2020.
- [24] Y. Gal and Z. Ghahramani, "Dropout as a bayesian approximation: Representing model uncertainty in deep learning," in *ICML*, vol. 48, 2016, pp. 1050–1059.
- [25] A. Graves, "Practical variational inference for neural networks," in *Adv Neural Inform Process Syst*, vol. 24, 2011, pp. 2348–2356.
- [26] T. Bui, D. Hernández-Lobato, J. Hernandez-Lobato *et al.*, "Deep Gaussian processes for regression using approximate expectation propagation," in *ICML*, 2016, pp. 1472–1481.
- [27] D. T. Mirikitani and N. Nikolaev, "Dynamic modeling with ensemble Kalman filter trained recurrent neural networks," in *7th ICMLA*. IEEE, 2008, pp. 843–848.
- [28] M. A. Maleki Sadr, J. Gante, B. Champagne *et al.*, "Uncertainty Estimation via Monte Carlo Dropout in CNN-based mmWave MIMO Localization," *IEEE Signal Process. Lett.*, pp. 1–1, 2021.
- [29] Y. Gal and Z. Ghahramani, "A theoretically grounded application of dropout in recurrent neural networks," *Adv. Neural Inf. Process. Syst.*, vol. 29, pp. 1019–1027, 2016.
- [30] L. Mou, L. Liang, Z. Gao *et al.*, "A multi-scale anomaly detection framework for retinal oct images based on the bayesian neural network," *Biomedical Signal Processing and Control*, vol. 75, p. 103619, 2022. [Online]. Available: <https://www.sciencedirect.com/science/article/pii/S1746809422001410>
- [31] J. Zraggen, G. Pizza, and L. G. Huber, "Uncertainty informed anomaly scores with deep learning: Robust fault detection with limited data," in *PHM Society European Conference*, vol. 7, no. 1, 2022, pp. 530–540.
- [32] D. Codetta-Raiteri and L. Portinale, "Dynamic bayesian networks for fault detection, identification, and recovery in autonomous spacecraft," *IEEE Transactions on Systems, Man, and Cybernetics: Systems*, vol. 45, no. 1, pp. 13–24, 2015.
- [33] W. Gao and Z.-H. Zhou, "Dropout rademacher complexity of deep neural networks," *Sci. China Inf. Sci.*, vol. 59, no. 7, pp. 1–12, 2016.
- [34] A. Bifet and R. Gavaldà, "Learning from time-changing data with adaptive windowing," in *Proceedings of the 2007 SIAM international conference on data mining*. SIAM, 2007, pp. 443–448.
- [35] S. Hochreiter and J. Schmidhuber, "Long short-term memory," *Neural Computation*, vol. 9, no. 8, pp. 1735–1780, 1997.
- [36] M. Mohri, A. Rostamizadeh, and A. Talwalkar, *Foundations of machine learning*. MIT press, 2018.

**Mohammad Amin Maleki Sadr** He received his B.Sc. degree from University of Isfahan, Iran, and the M.Sc., and Ph.D. degrees from K.N. Toosi University of Technology, Tehran, Iran in 2012, 2014, and 2018, respectively, all in Electrical Engineering. He is now a postdoc research fellow at Department of Statistics & Actuarial Science in University of Waterloo, Canada. His research interests include deep learning, anomaly detection, localization, signal processing, and wireless communication.



**Yeying Zhu** received her Ph.D. degree in Statistics from Pennsylvania State University, USA. She is currently an Associate Professor at Department of Statistics & Actuarial Science from University of Waterloo. Her research interest lies in the interface between causal inference and machine learning methods.

**Peng Hu** received his Ph.D. degree in Electrical Engineering from Queen's University, Canada. He is currently a Research Officer at the National Research Council Canada and an Adjunct Professor at the University of Waterloo. He has served as an associate editor of the Canadian Journal of Electrical and Computer Engineering, a member of the IEEE Sensors Standards committee, and on the organizing and technical committees of industry consortia and international conferences/workshops at IEEE ICC'23, IEEE PIMRC'17, IEEE AINA'15, etc. His current research interests include satellite-terrestrial integrated networks, autonomous networking, and industrial Internet of Things systems.